Acquisition and Analysis of Bispectral Bidirectional Reflectance Distribution Functions

Matthias B. Hullin[1] Boris Ajdin[1]
Johannes Hanika[2]
Hans-Peter Seidel[1] Jan Kautz[3]
Hendrik P. A. Lensch[2]

MPI–I–2009–4–001 July 2009

Authors' Addresses

[1]

Max-Planck-Institut für Informatik
Campus E1.4
66123 Saarbrücken
Germany

[2]

Institut für Medieninformatik
Universität Ulm
James-Franck-Ring
89081 Ulm
Germany

[3]

Dept. of Computer Science
University College London
Malet Place
London WC1E 6BT
United Kingdom

Acknowledgements

The authors would like to thank Michael Laise and Axel Koeppel for their technical support, and Karol Myszkowski for his valuable comments. This work has been partially funded by the DFG Emmy Noether fellowship (Le 1341/1-1) and the Max Planck Center for Visual Computing and Communication (BMBF-FKZ01IMC01).

Abstract

In fluorescent materials, energy from a certain band of incident wavelengths is reflected or reradiated at larger wavelengths, i.e. with lower energy per photon. While fluorescent materials are common in everyday life, they have received little attention in computer graphics. Especially, no bidirectional reflectance measurements of fluorescent materials have been available so far. In this paper, we develop the concept of a *bispectral BRDF*, which extends the well-known concept of the bidirectional reflectance distribution function (BRDF) to account for energy transfer between wavelengths. Using a bidirectional and bispectral measurement setup, we acquire reflectance data of a variety of fluorescent materials, including vehicle paints, paper and fabric. We show bispectral renderings of the measured data and compare them with reduced versions of the bispectral BRDF, including the traditional RGB vector valued BRDF. Principal component analysis of the measured data reveals that for some materials the fluorescent reradiation spectrum changes considerably over the range of directions. We further show that bispectral BRDFs can be efficiently acquired using an acquisition strategy based on principal components.

Keywords

fluorescent materials, bispectral BRDF

Contents

1 Introduction

Fluorescent materials change the wavelength of light upon reflection. This applies to many day-to-day materials, for instance human teeth, utility vehicle paints, detergents (fabric whiteners), or even ordinary photocopying paper. This shift of wavelength causes compelling visual effects if it occurs within the visible spectrum or turns UV radiation into visible light. In particular, many fluorescent surfaces appear brighter than perfectly white surfaces (Figure 1.2).

The physical foundations underlying this cross-wavelength energy transfer are well understood. A fluorescent medium consists of atoms or molecules that absorb incident photons at a given wavelength, and re-emit them after a short time (in the order of 10^{-8} s). During this short time interval, the electrons of the fluorescent molecule remain in an excited state above the ground energy level. The re-emission of a photon occurs when the fluorophore relaxes to its ground state. Due to mechanical interaction with the surrounding molecules, some of the excitation energy is lost during this process, leading to a change of wavelength, or Stokes shift. As required for conservation of energy, this shift always occurs towards larger wavelengths, corresponding to a loss in per-photon energy.

The wavelength-shifting behavior of a fluorescent material can be intuitively described *bispectrally* using a so-called *reradiation matrix*, specifying for each combination of incoming and outgoing wavelengths the amount of reradiated light. At the same time, however, the reflectance of every real-world material also depends on the directions of the incident and reflected light rays with regard to the surface, as usually described by the *bidirectional reflectance distribution function* (BRDF) [18]. In this paper, we extend this well-known concept to the *bispectral BRDF* that can describe general fluorescent materials and the bidirectional dependency of their wavelength-preserving and -shifting reflectance.

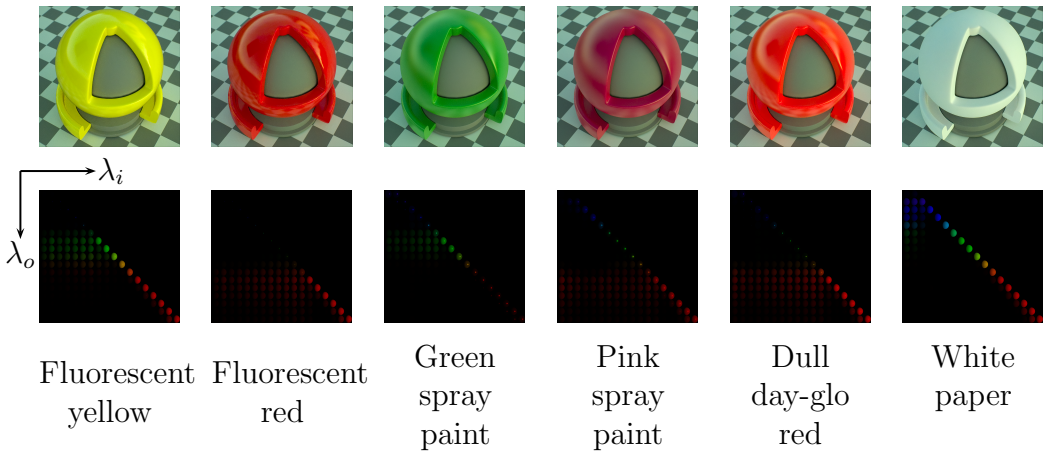

Figure 1.1: Fluorescent materials partially reflect or reradiate light at higher wavelength λ_o than the wavelength of the incoming light λ_i. Measured bispectral BRDFs capture this behavior as the renderings for various materials using a spectral environment map convey. In the bottom row we arrange slices of the bispectral BRDF, showing one rendered sphere for each pair of incident and reradiated wavelengths $(\lambda_o, \lambda_i) \in [400\,\text{nm}; 720\,\text{nm}] \times [380\,\text{nm}; 720\,\text{nm}]$. Fluorescence is represented by the off-diagonal entries.

While there have been attempts to approximate fluorescent materials with analytical models, to our knowledge the full bidirectional and bispectral reflectance of real materials has not been measured so far. By equipping a traditional BRDF measurement setup with spectral filters for light source and camera, we acquire bispectral BRDF datasets for a range of isotropic fluorescent materials.

Given the measured data, we project them into a sparse spectral basis using principal component analysis (PCA). The analysis reveals a non-trivial dependency of the fluorescent effect on the incident and reflection angle. Furthermore, such a decomposition, if performed on a partially acquired dataset, allows for efficient planning of the remaining acquisition task. Measuring the bispectral dependency using a sparse basis of wavelength combinations greatly reduces the measurement effort.

Figure 1.2: Spheres covered in three different paint varieties for utility vehicles ("pearl white" primer, fluorescent red/yellow/orange paint, clear coat). Note that the luminance of the orange and yellow spheres is higher than the one of the 90% white ColorChecker patch.

2 Related Work

Much work has been done in the area of reflectance acquisition. Starting in the early nineties, Ward [22] measured and modeled the BRDF of anisotropic materials. The first larger database of BRDFs is the CUReT database [4] with 61 different materials, albeit sampled sparsely. Matusik et al. [14] measure more than 100 different materials, using a similar setup to Marschner et al. [13], from which they derive a generative BRDF model. The above methods measure RGB reflectance distributions, but spectral measurement techniques are available too [20]. However, to the best of our knowledge, measurement of bispectral reflectance distributions has not been done. Only limited bispectral slices of BRDFs (fixed view and light) are commonly measured [8], which is often referred to as fluorescent colorimetry [25].

The less general case of spectral reflectances with fixed view/light configuration has been studied as well. For instance, spectral reflectance of skin has been measured [1]. Similarly, spectral imaging of skin has been used to determine skin appearance parameters [5]. Hersch et al. [9] measured the spectral response of fluorescent paints under UV illumination with fixed view/light directions.

Substantial work has also been done on analytical BRDF models, see Ngan et al. [17] for an overview of different models and how well they approximate BRDF measurements. Many of these BRDF models describe spectral reflectance distributions, such as the Cook-Torrance BRDF [3], but do not model bispectral distributions needed for fluorescence. In summary, none of the above research deals with bispectral BRDFs, i.e., reflectance data that depends on view and light direction as well as incident and outgoing wavelength.

A recent paper by Wilkie et al. [24] performs a qualitative analysis of a fluorescent material by visually examining the reflection of a green laser on an

orange fluorescent cardboard. The authors conclude that while fluorescence is mostly a diffuse effect, it may still depend on the view/light directions, e.g., due to additional Fresnel effects. Based on these insights, the authors hand-craft a fluorescent orange BRDF. Rather than deriving an analytic model, our goal is to acquire bispectral as well as bidirectional reflectances, which allows us to gain better understanding of fluorescent materials and to analyze the dependency of fluorescence on view and light directions. allows us to build a suitable BRDF model.

Glassner [7] was the first to adapt the rendering equation [12] to include fluorescence (as well as phosphorescence). In essence, reradiation from every incident wavelength to all possible outgoing wavelengths needs to be taken into account. It was later extended by Wilkie et al. [23] to include polarization.

3 Bispectral Reflectance

3.1 Bispectral Rendering Equation

Light transport considering energy transfer from one wavelength to another, in order to account for fluorescence, can be expressed by the bispectral rendering equation:

$$L(\omega_\mathrm{o}, \lambda_\mathrm{o}) = L_e(\omega_\mathrm{o}, \lambda_\mathrm{o}) + \int_\Omega \int_\Lambda L(\omega_\mathrm{i}, \lambda_\mathrm{i}) f_r(\omega_\mathrm{o}, \omega_\mathrm{i}, \lambda_\mathrm{o}, \lambda_\mathrm{i}) \mathrm{d}\lambda_\mathrm{i}\, \mathrm{d}\omega_\mathrm{i}, \quad (3.1)$$

which in contrast to the normal rendering equation [12] requires an additional integration over all incident wavelengths. Solving it is straightforward when using spectral path tracing, e.g. [2], but of course other rendering techniques can be adopted as well.

3.2 Bispectral BRDF

The rendering equation includes the *bispectral* BRDF $f_\mathrm{r}(\omega_\mathrm{o}, \omega_\mathrm{i}, \lambda_\mathrm{o}, \lambda_\mathrm{i})$ that describes the angularly dependent reflection for any pair of wavelengths.

The definition of the bispectral BRDF is different from the original definition of a spectral BRDF [18] which cannot represent fluorescent materials. Furthermore, it is more general than the proposed use of reradiation matrices [7], which assumes separability, i.e. that the relative fluorescent spectrum does not change with direction.

Before we derive the general *bispectral* BRDF let us briefly recall the definition of a *spectral* BRDF. The required spectral quantities are defined in Table 3.1. Note that the spectral quantities feature a different unit compared

Radiance	$L(\omega)$	$\left[\frac{\mathrm{W}}{\mathrm{sr}\cdot\mathrm{m}^2}\right]$
Spectral Radiance	$L(\omega,\lambda)$	$\left[\frac{\mathrm{W}}{\mathrm{sr}\cdot\mathrm{m}^2\cdot\mathrm{nm}}\right]$
Spectral Irradiance	$E(\lambda)=\int_\Omega L(\omega,\lambda)\mathrm{d}\omega$	$\left[\frac{\mathrm{W}}{\mathrm{m}^2\cdot\mathrm{nm}}\right]$
Irradiance	$E=\int_\Lambda\int_\Omega L(\omega,\lambda)\mathrm{d}\omega\ \mathrm{d}\lambda$	$\left[\frac{\mathrm{W}}{\mathrm{m}^2}\right]$

Table 3.1: Definitions of spectral quantities; ω refers to directions and λ to wavelengths.

to their non-spectral counterparts. Following Nicodemus et al. [18], the differential reflected spectral radiance $\mathrm{d}L_\mathrm{o}(\omega_\mathrm{o},\lambda_\mathrm{o})$ due to the incident differential spectral irradiance $\mathrm{d}E(\lambda)$ from direction ω_i is given as:

$$\mathrm{d}L_\mathrm{o}(\omega_\mathrm{o},\lambda)=\mathrm{d}E(\lambda)f_\mathrm{r}(\omega_\mathrm{o},\omega_\mathrm{i},\lambda)\quad\left[\frac{\mathrm{W}}{\mathrm{sr}\cdot\mathrm{m}^2\cdot\mathrm{nm}}\right], \tag{3.2}$$

with ω_i and ω_o being the incident and outgoing directions. The spectral BRDF $f_\mathrm{r}(\omega_\mathrm{o},\omega_\mathrm{i},\lambda)$ for a single wavelength is therefore defined as the ratio of differential reflected spectral radiance to differential incident spectral irradiance:

$$f_\mathrm{r}(\omega_\mathrm{o},\omega_\mathrm{i},\lambda)=\frac{\mathrm{d}L_\mathrm{o}(\omega_\mathrm{o},\lambda)}{\mathrm{d}E(\lambda)}=\frac{\mathrm{d}L_\mathrm{o}(\omega_\mathrm{o},\lambda)}{L_\mathrm{i}(\omega_\mathrm{i},\lambda)\cos(\theta_\mathrm{i})\mathrm{d}\omega_\mathrm{i}}\quad\left[\frac{1}{\mathrm{sr}}\right]. \tag{3.3}$$

It follows that the unit of the spectral BRDF is $\left[\frac{1}{sr}\right]$, which is the same as for non-wavelength dependent BRDFs $f_\mathrm{r}(\omega_\mathrm{o},\omega_\mathrm{i})$, although the units for L and E differ in the spectral vs. non-spectral case.

The unit of the *bispectral* BRDF however is different as we will show in the following. We generalize Nicodemus' derivation of the BRDF to account for cross-wavelength energy transfer by the bispectral BRDF: Referring to the bispectral rendering equation (Eq.3.1) the double differential spectral radiance (differential with regard to the incident direction ω_i *and* the incident wavelength λ_i) is due to incident double differential *(non-spectral)* irradiance for ω_i and λ_i:

$$\mathrm{d}^2L_\mathrm{o}(\omega_\mathrm{o},\lambda_\mathrm{o})=\mathrm{d}^2E\cdot f_\mathrm{r}(\omega_\mathrm{o},\omega_\mathrm{i},\lambda_\mathrm{o},\lambda_\mathrm{i})\quad\left[\frac{\mathrm{W}}{\mathrm{sr}\cdot\mathrm{m}^2\cdot\mathrm{nm}}\right], \tag{3.4}$$

and hence the *bispectral BRDF* may be defined as

$$f_\mathrm{r}(\omega_\mathrm{o},\omega_\mathrm{i},\lambda_\mathrm{o},\lambda_\mathrm{i})=\frac{\mathrm{d}^2L_\mathrm{o}(\omega_\mathrm{o},\lambda_\mathrm{o})}{L_\mathrm{i}(\omega_\mathrm{i},\lambda_\mathrm{i})\cos(\theta_\mathrm{i})\mathrm{d}\omega_\mathrm{i}\,\mathrm{d}\lambda_\mathrm{i}}\quad\left[\frac{1}{\mathrm{sr}\cdot\mathrm{nm}}\right]. \tag{3.5}$$

The bispectral BRDF is a general way to represent fluorescent materials as it does not make any assumptions about the material.

In the discretized case, an individual sample of the bispectral BRDF for the directions $(\omega_\mathrm{i}, \omega_\mathrm{o})$ expresses the energy transfer from the incoming spectrum to the reflected spectrum as a matrix over $\lambda_\mathrm{o}, \lambda_\mathrm{i}$, see Figure 1.1. While the diagonal entries refer to reflection at the same wavelength, the fluorescent effect is represented by the off-diagonal part. As there is typically no transfer from longer to shorter wavelengths (towards higher energy) the upper triangle will remain black.

4 Measurement and Reconstruction

In order to acquire isotropic bispectral BRDFs, we have built an image-based measurement device. samples were isotropic, Our device follows the design of Matusik et al. [14] for isotropic BRDFs but with the added capability to emit and acquire at specific wavelength bands.

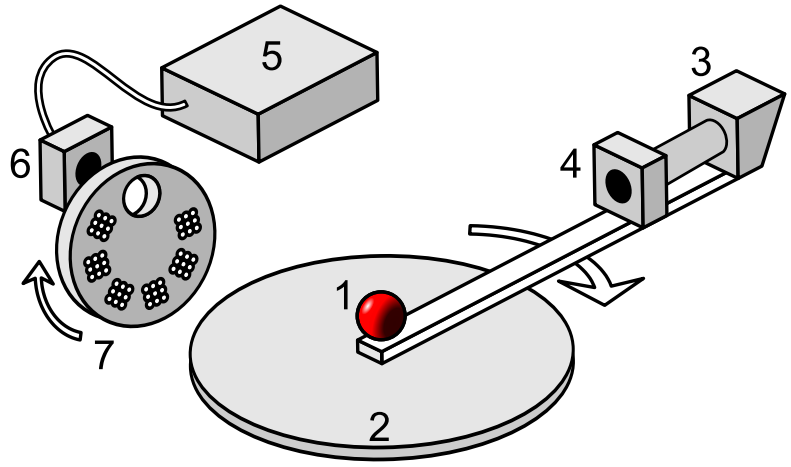

Figure 4.1: A depiction of our setup. A sample sphere (1) is mounted on a turn table (2), to which a digital monochrome still camera (3) is attached. The camera is equipped with a visible-spectrum tunable filter (4). The sphere is illuminated by a light guide coupled xenon light source (5) with another tunable filter (6) mounted in front; UV light is generated with UV LEDs that can be selected using a motorized wheel (7).

4.1 Setup

Our measurement setup is depicted in Figure 4.1. This fully automated device consists of a light source and a camera, both of which can be tuned spectrally to emit or measure a rather narrow spectral band around a single selected wavelength. Using a turn table, the relative position of camera and light source can be controlled.

The spectral filters used are LCD-based Lyot filters (CRi VariSpec VIS10 35 mm) whose transmission bands are about 10 nm–20 nm wide and range from 400 nm to 720 nm. As light source we employ a xenon arc lamp coupled into a light fiber (XION medical Xenon R180), whose light has a rather flat and stable spectrum but rather little blue and UV output, especially after passing the spectral filter. We therefore add LEDs for better coverage of this range (370 nm–420 nm in 10 nm steps). The camera is a monochrome, digital still camera (Jenoptik ProgRes MFcool), with which we acquire high-dynamic-range images using exposure series from 1 ms to 16 s.

For all of the components, the spectral transmission or sensitivity curves have been either obtained from the manufacturers or calibrated using a photospectrometer. The absolute scaling is determined by measuring a Spectralon target, which preserves the wavelength and has a well-defined reflectance (99% quasi-Lambertian reflectivity across the spectrum), i.e. the rows of the captured Spectralon bispectral BRDF sample have to add up to $0.99\,\mathrm{sr}^{-1}$. We obtain a specific spectral scaling factor $s(\lambda_\mathrm{o}, \lambda_\mathrm{i})$ for each wavelength pair. Any captured camera value is scaled according to $s(\lambda_\mathrm{o}, \lambda_\mathrm{i})$ before generating one entry in the matrix of a bispectral BRDF sample.

4.2 Measurement and data processing

The standard acquisition of a bispectral BRDF consists of capturing images of the material sampled at different turn table rotations β for every pair of wavelengths $(\lambda_\mathrm{o}, \lambda_\mathrm{i})$. For practical reasons we limited ourselves to steps of 20 nm in the range from 380 nm to 720 nm for λ_i and 400 nm to 720 nm for λ_o amounting to 170 images per β as the upper triangle of the bispectral matrix can be ignored. We vary β in the range of 5° to 170°. For highly specular materials a stepping of 1° is chosen to sufficiently sample the sharp highlight while we take a coarser sampling of 20° for close to diffuse materials. The acquisition is followed by geometric processing and resampling.

Adaptive Measurement. In the case of a PCA-steered measurement (Section 6), we first acquire full bispectral datasets for a small number of angles. After performing the PCA decomposition, we acquire dense angular data only for the sparse bispectral basis required for a good reconstruction.

Geometric processing. Depending on the material, we use two different sample geometries: coated spheres for the paints and a custom-made piecewise cylindrical object (Figure 8.2) wrapped in stripes of paper or fabric.

Due to the varying normals of the shapes each surface point will be illuminated and viewed from a slightly different direction. After a simple geometric calibration of the setup and the sample we can determine $(\omega_\mathrm{o}, \omega_\mathrm{i})$ for every pixel captured under a specific turn table rotation β.

For storage and further processing, we discretize the data for each wavelength pair in 32^3 bins using the $(\theta_\mathrm{o}, \theta_\mathrm{i}, \phi_\mathrm{diff})$ parameterization chosen in [14]. For the strongly specular materials, 64^3 bins are used. Since the coarse sampling of the turn table position does not necessarily populate all bins, the missing data are filled using diffusion.

During rendering a specific reflectance sample $f_r(\theta_\mathrm{o}, \theta_\mathrm{i}, \phi_\mathrm{diff}, \lambda_\mathrm{o}, \lambda_\mathrm{i})$ is obtained by multilinear interpolation from our bispectral BRDF representation.

5 Data Analysis

Previous work assumes separability of directions and wavelengths into a BRDF and a single reradiation matrix [7, 24]. In order to test separability, we have factored our bispectral BRDFs using principal component analysis:

$$f_r(\omega_\mathrm{o}, \omega_\mathrm{i}, \lambda_\mathrm{o}, \lambda_\mathrm{i}) \approx \sum_k f_k(\omega_\mathrm{o}, \omega_\mathrm{i}) \cdot p_k(\lambda_\mathrm{o}, \lambda_\mathrm{i}). \tag{5.1}$$

The PCA is computed on the matrix formed by the BRDF samples where the directions $(\omega_\mathrm{o}, \omega_\mathrm{i})$ and the bispectral dimension $(\lambda_\mathrm{o}, \lambda_\mathrm{i})$ are flattened into the row and column indices, respectively. We obtain principle components that represent the space of reradiation matrices.

For the analysis, we remove the diagonal and 2^{nd}-diagonal ($\lambda_\mathrm{o} \approx \lambda_\mathrm{i}$) from all bispectral BRDF samples, which contain many highlight samples. This prevents highlights from influencing the analysis, as we are only interested in the separability of fluorescent effects and not of highlights. We have factored all bispectral BRDFs that we measured and found that the number of terms required to reconstruct the BRDF to a reasonable fidelity (capturing 98% of the variance) varies considerably. The result for three interesting fluorescent BRDFs is shown in Figure 5.1. Fluorescent red and fluorescent yellow require four and three terms respectively to achieve this fidelity, whereas paper can be approximated well even with a single term. Figure 5.1 shows Fluorescent Red under blue illumination and it is obvious that one term is not sufficient, whereas three terms are visually sufficient (capturing almost 98% of variance). This confirms that there are directionally dependent fluorescent effects in certain materials. Both fluorescent red and yellow are coated, which suggests Fresnel effects to be a likely cause of this dependence.

(a)

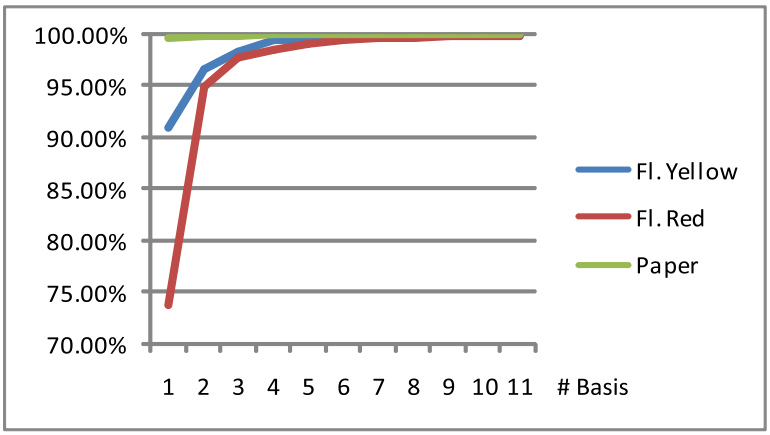

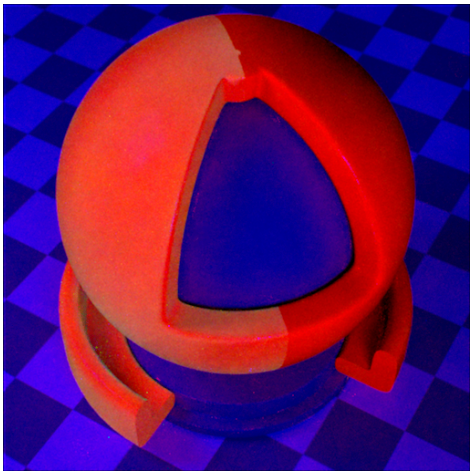

(b) 1 Basis

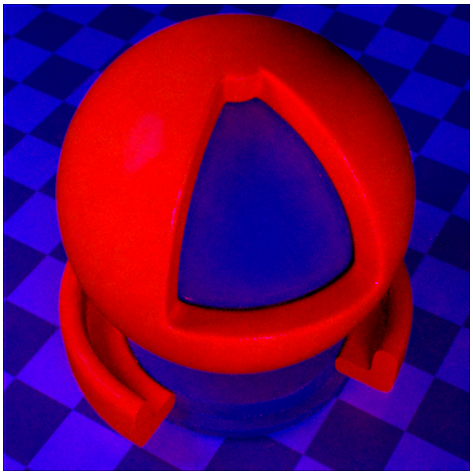

(c) 5 Bases

Figure 5.1: The graph (a) depicts how many PCA bases are required to reconstruct a bispectral BRDF to a certain fidelity (i.e., to capture N% of variance). For most materials more than one term is required to achieve reasonable quality, confirming that fluorescent effects can be directionally dependent. At the bottom you can see a rendering using one basis (b) and using five bases (c), confirming numerical results (the sphere is split, the right side is original BRDF).

6 PCA-based Acquisition

The insights of the previous section indicate that rather few principal components suffice to faithfully represent all bispectral samples of a BRDF. We now analyze how this insight can be used to minimize the acquisition effort.

Our approach is similar to Matusik et al. [15] who reduced the number of samples for BRDF measurement based on the PCA over the full set of BRDFs in their database. As no bispectral BRDF database exists so far, we concentrate on the PCA of each individual bispectral BRDF.

In contrast to the previous section we now compute the PCA on the full bispectral matrix including the diagonal and 2^{nd}-diagonal as we now focus on the full bispectral BRDF rather than only on the fluorescence. For the accelerated acquisition we first acquire full bispectral measurements for three turn table angles β. As the exact selection of angles hardly influenced the PCA we picked $0°$, $70°$ and $150°$. Each acquired measurement contains a manifold of BRDF samples and the three angles together are likely to span the full range of possible samples. We compute the SVD of the matrix F representing all BRDF samples after subtracting the average of all samples $\bar{f}$. Selecting the n eigenvectors with the largest eigenvalues the basis B is assembled.

In order to project a yet to be measured sample uniquely into the basis we have to acquire at least n wavelength pairs $(\lambda_\text{o}, \lambda_\text{i})_k$ as we cannot illuminate with the basis vectors directly. The basis coefficients for a bispectral BRDF sample f are estimated from the sparse measurement $f' = \{f_k(\lambda_\text{o}, \lambda_\text{i})\}$ using the projection matrix P^+ so that f is approximated by

$$f \approx BP^+(f' - \bar{f}) + \bar{f}. \tag{6.1}$$

P^+ is the pseudo-inverse of P which in turn is composed of the subset of rows of B corresponding to $(\lambda_\text{o}, \lambda_\text{i})_k$. The selection of $(\lambda_\text{o}, \lambda_\text{i})_k$ influences

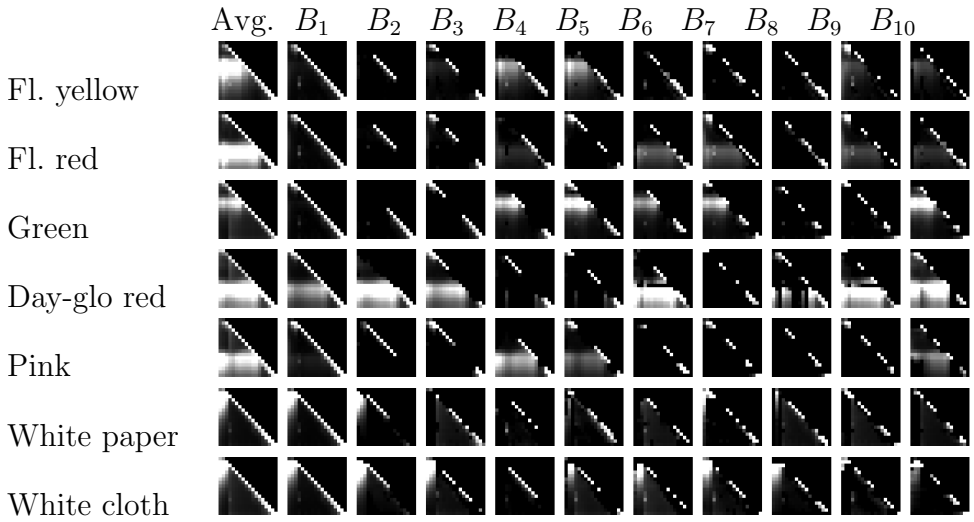

Figure 6.1: Average and the first 10 principal components B_i.

the stability of the approximation which is correlated to the condition number of P. Starting with the wavelength pair corresponding to the largest entry in B, we follow a greedy strategy selecting the set which brings cond(P) closest to 1.

6.1 Acquisition Results

The first ten basis vectors B for some of the captured materials are visualized in Figure 6.1. The corresponding development of eigenvalues is very similar to the plot in Figure 5.1(a). A noteworthy observation is that only White paper, Cloth and Day-glo red (the least specular samples) contain significant off-diagonal, i.e. fluorescent contributions in the first eigenvector. The eigenvalues indicate that the bispectral BRDFs of these materials can in fact be separated into a reradiation matrix and a BRDF. The other more specular materials first address the variation along the diagonal, i.e. the direct surface reflection, before exploring the variation in the off-diagonal part, indicating that the direction dependence of the fluorescence is coupled to the glossiness.

Based on the PCA we acquired the Pink dataset (Figure 1.1) using only 20 wavelength pairs while presumably even fewer would suffice. The reconstructed samples feature less noise as directly recorded samples since they are computed as a linear combination of multiple measurements. Including measurement of the whole bispectral matrix for angles 0°, 70°, 150° (4:30 h)

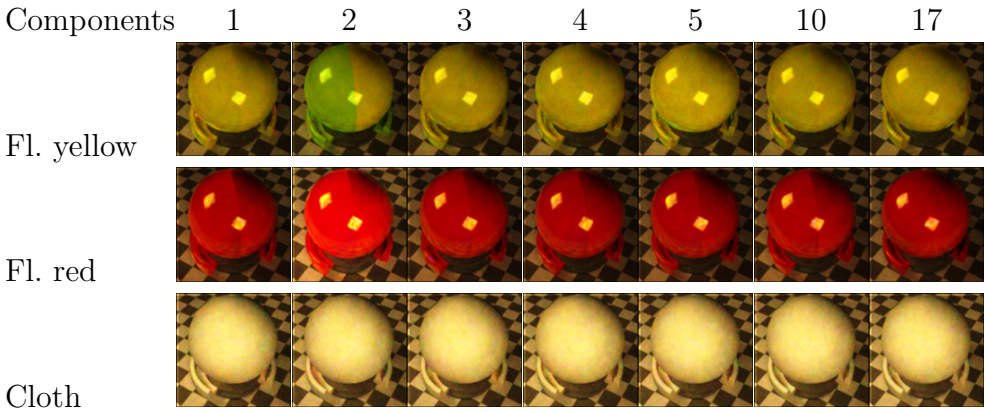

Figure 6.2: Quality of the reconstruction from varying numbers of acquired bispectral samples. Note the edge between the reconstructed bispectral BRDF on the left and the ground truth on the right half of the sphere.

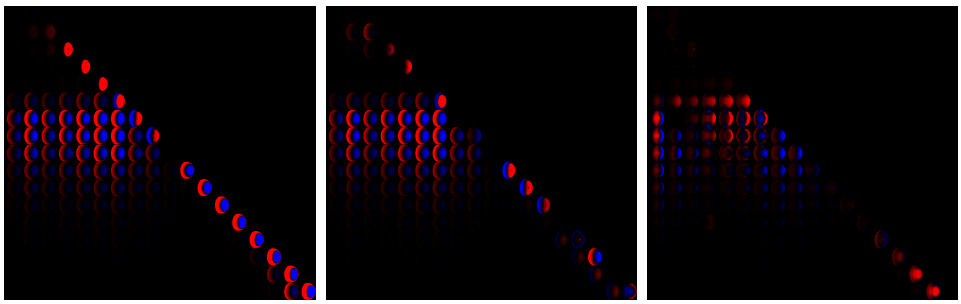

Figure 6.3: Difference between the reconstruction using 1,5, and 17 components on the Yellow data set (red - positive). The last image is brightened by a factor of 10 for visualization. Note the resemblance to higher-order spherical harmonics, implying a nontrivial angular dependency of reflectance.

the total acquisition time for 30 different angles was reduced to 9.5 h, i.e. 10 min per additional angle, compared to 45 h for a complete measurement.

Figure 6.2 analyzes the dependency of the reconstruction quality on the number of measured wavelength pairs. For the Cloth material after one sample the reconstructed bispectral BRDF is already hardly distinguishable from the ground truth. For the highly specular Yellow and Red, ten or more principal components are necessary to leverage any difference. Note the faulty green reflection in the yellow BRDF if too few samples are recorded. Figure 6.3 furthermore shows that the difference is actually strongly directionally dependent as the positive (red) and negative (blue) values show a strong correlation on the spheres for each (λ_o, λ_i).

7 Results

Using our measurement device, we have captured the bispectral BRDF of a number of fluorescent materials including fluorescent paints with or without a clear coating as well as paper and white cloth. As shown in Figure 1.1, the exciting wavelength as well as emittance fluorescence vary drastically between these materials.

The strength of the reradiation therefore depends heavily on the illuminating spectrum as demonstrated in Figure 8.1 and Figure 8.2. In Figure 8.2 RGB photographs are compared against renderings under a 5600K illuminant. As our acquisition system contains some UV LEDs, we can even capture materials such as the paper sample which exhibit significant reradiation in the blue to UV range. The effect is clearly visible in Figure 8.1. Our captured bispectral BRDFs faithfully reproduce the fluorescence in both images. Only the color of the Yellow sample and the paper slightly deviates in Figure 8.2 which we attribute to a different white balancing in the camera.

In Figure 8.4 we demonstrate that fluorescence does in fact require bispectral modeling of sufficient resolution. After reducing the measured bispectral BRDF samples to a 3×3 (RGB×RGB) matrix by integrating over the RGB spectral curves, the renderings show clear differences to the full bispectral BRDFs. Especially for the Yellow sample, the coarse RGB×RGB representation is unable to reproduce reradiation, which is sharply centered around 540nm. Ignoring fluorescence completely by converting the bispectral BRDF into a spectral BRDF (we assume a uniform illumination spectrum for the conversion), also shows some differences. They are less pronounced because the illumination in this scene is similar to the spectrum used for the conversion, however slight deviations in color and intensity can still be made out. Reducing the bispectral BRDF to a simple RGB BRDF (again assuming a uniform incident spectrum) shows obvious differences. These differences are most pronounced for non-white spectra as demonstrated in Figure 8.3.

8 Conclusion

Fluorescent materials transfer energy across different wavelength bands. We have introduced the definition of the bispectral BRDF, which enables us to model directionally-dependent fluorescent behavior. We have presented a measurement setup to acquire bispectral BRDFs, including a PCA-based acquisition method that only acquires relevant bispectral samples of the BRDF yielding a significant acquisition speedup.

We have analyzed the angular dependence of fluorescence on a number of materials, the analysis shows that for our glossy and specular materials, the resulting spectral distribution due to fluorescence changes with illumination and viewing direction. However, only a low number of principal components is required to represent this dependence. While this effect seems to be correlated to the Fresnel term a more thorough analysis is planned for the future.

Another extension is to improve our measurement setup. It currently employs tunable spectral filters which only let through a single wavelength band. Using a hyperspectral light source and camera, one would be able to directly sense the PC coefficients by illumination with the PCA basis vector rather than sensing individual wavelength pairs. Furthermore, compressed sensing in the wavelength domain could largely reduce the acquisition time.

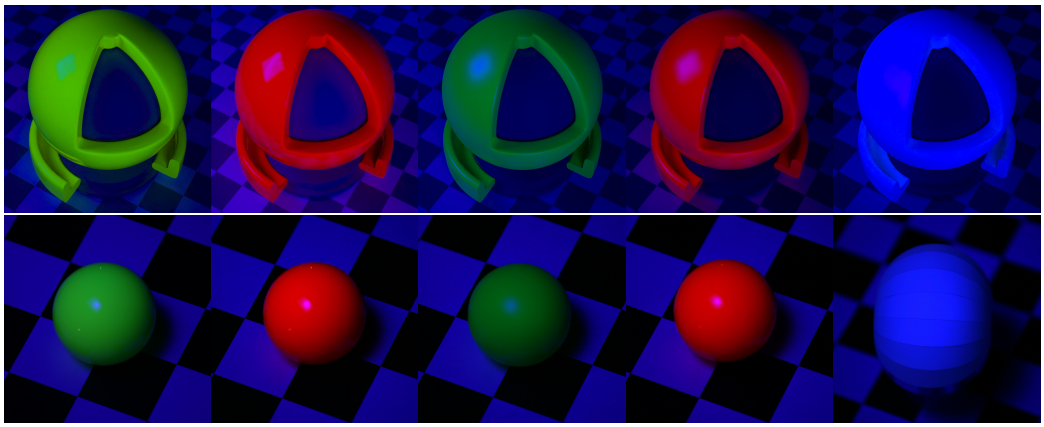

(a) Yell. (b) Red (c) Green (d) DullR (e) Paper

Figure 8.1: Renderings (top row) and photos (bottom row) of different materials under UV light (400 nm).

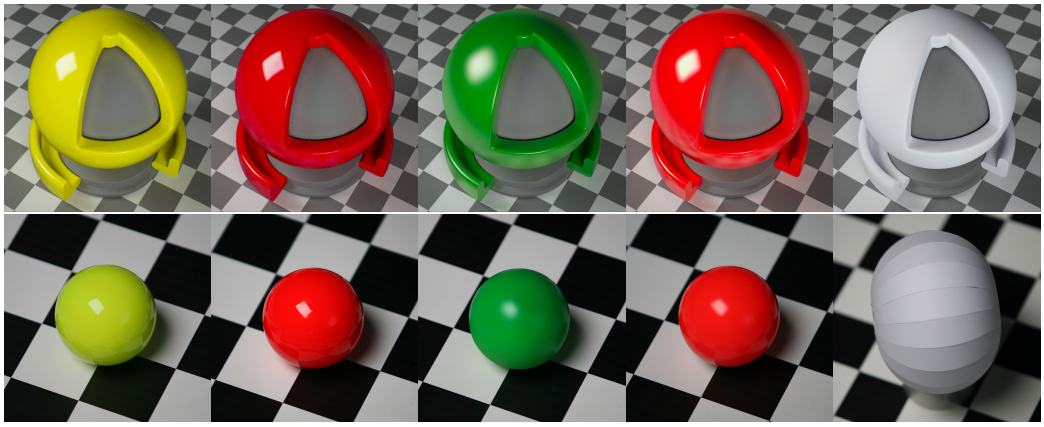

(a) Yell. (b) Red (c) Green (d) DullR (e) Paper

Figure 8.2: Renderings (top row) and photos (bottom row) of different materials under 5600K illumination. Slight variation is observed for Yellow and Paper which might be due to white balancing of the camera.

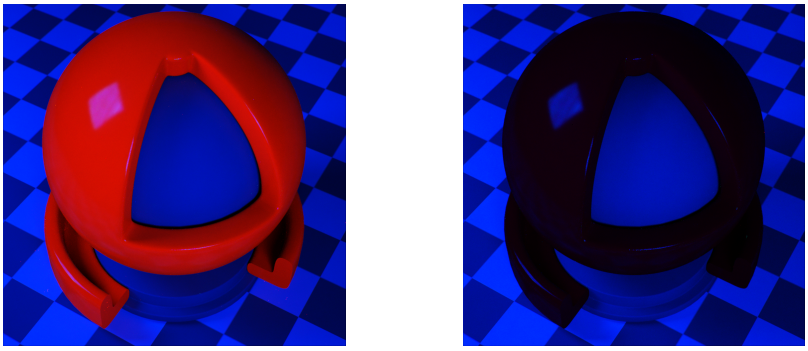

(a) bispectral BRDF (b) RGB BRDF

Figure 8.3: Measured Fluorescent red bispectral BRDF (a) compared to a simple RGB vector valued BRDF (b) under blue illumination. Note the cross-color reflectance from blue to red in the case of the full bispectral BRDF. The RGB BRDF cannot represent these complex color shifts and fails to reproduce the fluorescent effect.

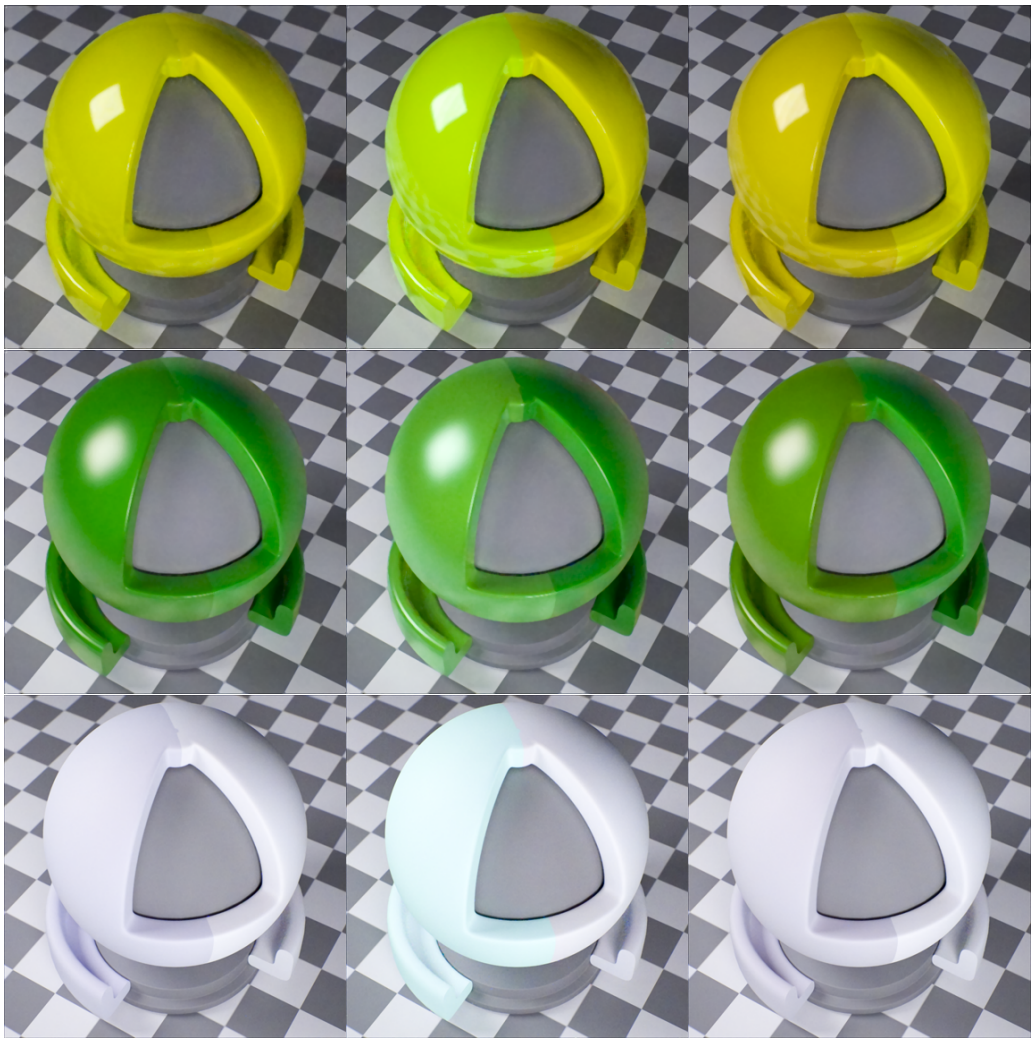

(a) Spectral (16 wavel.) (b) RGB 3×3 (c) RGB

Figure 8.4: Comparison renderings using 3 different measured fluorescent materials. Full bispectral BRDF measurements (right half of each sphere) are compared to: spectral measurements, RGB reradiation matrices, and standard RGB BRDFs.

Bibliography

[1] E. Angelopoulou and R. Molana. Multispectral skin color modeling. In *IEEE Conference on Computer Vision and Pattern Recognition*, pages 635–642, 2001.

[2] M. Bendig, J. Hanika, H. Dammertz, J. C. Goldschmidt, M. Peters, and M. Weber. Simulation of fluorescent concentrators. In *IEEE Symposium on Interactive Ray Tracing*, pages 93–98, Aug. 2008.

[3] R. Cook and K. Torrance. A reflectance model for computer graphics. In *SIGGRAPH*, pages 307–316, 1981.

[4] CUReT. Columbia Utrecht Texture Database. Web-Page. http://www1.cs.columbia.edu/CAVE/software/curet/index.php, 1996.

[5] C. Donner, T. Weyrich, E. d'Eon, R. Ramamoorthi, and S. Rusinkiewicz. A layered, heterogeneous reflectance model for acquiring and rendering human skin. *ACM Trans. Graph.*, 27(5):1–12, 2008.

[6] N. Gat. Imaging spectroscopy using tunable filters: A review. In H. H. Szu, M. Vetterli, W. J. Campbell, and J. R. Buss, editors, *SPIE Conference Series*, volume 4056, pages 50–64, Apr. 2000.

[7] A. Glassner. A Model for Fluorescence and Phosphorescence. In *Proceedings of the 5th Eurographics Workshop on Rendering*, pages 57–68, June 1994.

[8] D. Gundlach and H. Terstiege. Problems in measurement of fluorescent materials. *Color Research & Application*, 19(6):427–436, 1994.

[9] R. D. Hersch, P. Donzé, and S. Chosson. Color images visible under UV light. *ACM Trans. Graph. (Proc. SIGGRAPH)*, 26(3):75, 2007.

[10] S. Hordley, G. Finalyson, and P. Morovic. A multi-spectral image database and its application to image rendering across illumination. In *Proceedings of the Third International Conference on Image and Graphics*, pages 394–397, 2004.

[11] L. Huang, V. Catalano, and S.-W. Tam-Chang. Anisotropic fluorescent materials via self-organization of perylenedicarboximide. *Chemical Communications*, pages 2016–2018, 2007.

[12] J. Kajiya. The Rendering Equation. In *Computer Graphics (Proc. of SIGGRAPH '86)*, pages 143–150, August 1986.

[13] S. Marschner, S. Westin, E. Lafortune, and K. Torrance. Image-based bidirectional reflectance distribution function measurement. *Applied Optics*, 39(16):2592–2600, 2000.

[14] W. Matusik, H. Pfister, M. Brand, and L. McMillan. A data-driven reflectance model. *ACM Trans. Graph. (Proc. SIGGRAPH)*, 22(3):759–769, 2003.

[15] W. Matusik, H. Pfister, M. Brand, and L. McMillan. Efficient isotropic BRDF measurement. In *Eurographics Symposium on Rendering: 14th Eurographics Workshop on Rendering*, pages 241–248, June 2003.

[16] H. H. Muhammed, P. Ammenberg, and E. Bengtsson. Using feature-vector based analysis, based on principal component analysis and independent component analysis, for analyzing hyperspectral images. In *Proceedings of the 11th International Conference on Image Analysis and Processing*, pages 309–315, 2001.

[17] A. Ngan, F. Durand, and W. Matusik. Experimental analysis of BRDF models. In *Eurographics Symposium on Rendering*, pages 117–226, 2005.

[18] F. Nicodemus, J. Richmond, J. Hsia, I. Ginsberg, and T. Limperis. Geometrical considerations and nomenclature for reflectance. *Final Report, National Bureau of Standards, Washington, DC. Inst. for Basic Standards*, 1977.

[19] M. S. Peercy. Linear color representations for full spectral rendering. In *SIGGRAPH '93*, pages 191–198, 1993.

[20] J. Proctor and Y. Barnes. NIST high accuracy reference reflectometer-spectrophotometer. *Journal of Research of the National Institute of Standards and Technology*, 101(5):619–626, 1996.

[21] G. Rougeron and B. Peroche. An adaptive representation of spectral data for reflectance computations. In *Proceedings of the Eurographics Workshop on Rendering*, pages 127–138, 1997.

[22] G. J. Ward. Measuring and modeling anisotropic reflection. *Computer Graphics (Proc. SIGGRAPH)*, 26(2):265–272, 1992.

[23] A. Wilkie, R. Tobler, and W. Purgathofer. Combined rendering of polarization and fluorescence effects. In *Proceedings of the 12th Eurographics Workshop on Rendering*, pages 197–204, 2001.

[24] A. Wilkie, A. Weidlich, C. Larboulette, and W. Purgathofer. A reflectance model for diffuse fluorescent surfaces. In *Proceedings of Graphite 2006*, pages 321–328, 11 2006.

[25] G. Wyszecki and W. S. Stiles. *Color Science: Concepts and Methods, Quantitative Data and Formulae*. John Wiley and Sons, New York, 1982.

[26] A. Zastrow. Physikalische Analyse der Energieverlustmechanismen im Fluoreszenzkollektor. *PhD thesis, Albert-Ludwigs-Universität Freiburg, Germany, 1981*, 1981.

Below you find a list of the most recent technical reports of the Max-Planck-Institut für Informatik. They are available via WWW using the URL `http://www.mpi-inf.mpg.de`. If you have any questions concerning WWW access, please contact `reports@mpi-inf.mpg.de`. Paper copies (which are not necessarily free of charge) can be ordered either by regular mail or by e-mail at the address below.

Max-Planck-Institut für Informatik
Library
attn. Anja Becker
Stuhlsatzenhausweg 85
66123 Saarbrücken
GERMANY
e-mail: `library@mpi-inf.mpg.de`

MPI-I-2009-RG1-002	P. Wischnewski, C. Weidenbach	Contextual rewriting
MPI-I-2009-5-006	S. Bedathur, K. Berberich, J. Dittrich, N. Mamoulis, G. Weikum	Scalable phrase mining for ad-hoc text analytics
MPI-I-2009-5-004	N. Preda, F.M. Suchanek, G. Kasneci, T. Neumann, G. Weikum	Coupling knowledge bases and web services for active knowledge
MPI-I-2009-5-003	T. Neumann, G. Weikum	The RDF-3X engine for scalable management of RDF data
MPI-I-2008-RG1-001	A. Fietzke, C. Weidenbach	Labelled splitting
MPI-I-2008-5-004	F. Suchanek, M. Sozio, G. Weikum	SOFI: a self-organizing framework for information extraction
MPI-I-2008-5-003	F.M. Suchanek, G. de Melo, A. Pease	Integrating Yago into the suggested upper merged ontology
MPI-I-2008-5-002	T. Neumann, G. Moerkotte	Single phase construction of optimal DAG-structured QEPs
MPI-I-2008-5-001	F. Suchanek, G. Kasneci, M. Ramanath, M. Sozio, G. Weikum	STAR: Steiner tree approximation in relationship-graphs
MPI-I-2008-4-003	T. Schultz, H. Theisel, H. Seidel	Crease surfaces: from theory to extraction and application to diffusion tensor MRI
MPI-I-2008-4-002	W. Saleem, D. Wang, A. Belyaev, H. Seidel	Estimating complexity of 3D shapes using view similarity
MPI-I-2008-1-001	D. Ajwani, I. Malinger, U. Meyer, S. Toledo	Characterizing the performance of Flash memory storage devices and its impact on algorithm design
MPI-I-2007-RG1-002	T. Hillenbrand, C. Weidenbach	Superposition for finite domains
MPI-I-2007-5-003	F.M. Suchanek, G. Kasneci, G. Weikum	Yago : a large ontology from Wikipedia and WordNet
MPI-I-2007-5-002	K. Berberich, S. Bedathur, T. Neumann, G. Weikum	A time machine for text search
MPI-I-2007-5-001	G. Kasneci, F.M. Suchanek, G. Ifrim, M. Ramanath, G. Weikum	NAGA: searching and ranking knowledge
MPI-I-2007-4-008	J. Gall, T. Brox, B. Rosenhahn, H. Seidel	Global stochastic optimization for robust and accurate human motion capture

MPI-I-2007-4-007	R. Herzog, V. Havran, K. Myszkowski, H. Seidel	Global illumination using photon ray splatting
MPI-I-2007-4-006	C. Dyken, G. Ziegler, C. Theobalt, H. Seidel	GPU marching cubes on shader model 3.0 and 4.0
MPI-I-2007-4-005	T. Schultz, J. Weickert, H. Seidel	A higher-order structure tensor
MPI-I-2007-4-004	C. Stoll, E. de Aguiar, C. Theobalt, H. Seidel	A volumetric approach to interactive shape editing
MPI-I-2007-4-003	R. Bargmann, V. Blanz, H. Seidel	A nonlinear viseme model for triphone-based speech synthesis
MPI-I-2007-4-002	T. Langer, H. Seidel	Construction of smooth maps with mean value coordinates
MPI-I-2007-4-001	J. Gall, B. Rosenhahn, H. Seidel	Clustered stochastic optimization for object recognition and pose estimation
MPI-I-2007-2-001	A. Podelski, S. Wagner	A method and a tool for automatic veriication of region stability for hybrid systems
MPI-I-2007-1-003	A. Gidenstam, M. Papatriantafilou	LFthreads: a lock-free thread library
MPI-I-2007-1-002	E. Althaus, S. Canzar	A Lagrangian relaxation approach for the multiple sequence alignment problem
MPI-I-2007-1-001	E. Berberich, L. Kettner	Linear-time reordering in a sweep-line algorithm for algebraic curves intersecting in a common point
MPI-I-2006-5-006	G. Kasnec, F.M. Suchanek, G. Weikum	Yago - a core of semantic knowledge
MPI-I-2006-5-005	R. Angelova, S. Siersdorfer	A neighborhood-based approach for clustering of linked document collections
MPI-I-2006-5-004	F. Suchanek, G. Ifrim, G. Weikum	Combining linguistic and statistical analysis to extract relations from web documents
MPI-I-2006-5-003	V. Scholz, M. Magnor	Garment texture editing in monocular video sequences based on color-coded printing patterns
MPI-I-2006-5-002	H. Bast, D. Majumdar, R. Schenkel, M. Theobald, G. Weikum	IO-Top-k: index-access optimized top-k query processing
MPI-I-2006-5-001	M. Bender, S. Michel, G. Weikum, P. Triantafilou	Overlap-aware global df estimation in distributed information retrieval systems
MPI-I-2006-4-010	A. Belyaev, T. Langer, H. Seidel	Mean value coordinates for arbitrary spherical polygons and polyhedra in $\mathbb{R}^3$
MPI-I-2006-4-009	J. Gall, J. Potthoff, B. Rosenhahn, C. Schnoerr, H. Seidel	Interacting and annealing particle filters: mathematics and a recipe for applications
MPI-I-2006-4-008	I. Albrecht, M. Kipp, M. Neff, H. Seidel	Gesture modeling and animation by imitation
MPI-I-2006-4-007	O. Schall, A. Belyaev, H. Seidel	Feature-preserving non-local denoising of static and time-varying range data
MPI-I-2006-4-006	C. Theobalt, N. Ahmed, H. Lensch, M. Magnor, H. Seidel	Enhanced dynamic reflectometry for relightable free-viewpoint video
MPI-I-2006-4-005	A. Belyaev, H. Seidel, S. Yoshizawa	Skeleton-driven laplacian mesh deformations

MPI-I-2006-4-004	V. Havran, R. Herzog, H. Seidel	On fast construction of spatial hierarchies for ray tracing
MPI-I-2006-4-003	E. de Aguiar, R. Zayer, C. Theobalt, M. Magnor, H. Seidel	A framework for natural animation of digitized models
MPI-I-2006-4-002	G. Ziegler, A. Tevs, C. Theobalt, H. Seidel	GPU point list generation through histogram pyramids
MPI-I-2006-4-001	A. Efremov, R. Mantiuk, K. Myszkowski, H. Seidel	Design and evaluation of backward compatible high dynamic range video compression
MPI-I-2006-2-001	T. Wies, V. Kuncak, K. Zee, A. Podelski, M. Rinard	On verifying complex properties using symbolic shape analysis
MPI-I-2006-1-007	H. Bast, I. Weber, C.W. Mortensen	Output-sensitive autocompletion search
MPI-I-2006-1-006	M. Kerber	Division-free computation of subresultants using bezout matrices
MPI-I-2006-1-005	A. Eigenwillig, L. Kettner, N. Wolpert	Snap rounding of Bézier curves
MPI-I-2006-1-004	S. Funke, S. Laue, R. Naujoks, L. Zvi	Power assignment problems in wireless communication
MPI-I-2005-5-002	S. Siersdorfer, G. Weikum	Automated retraining methods for document classification and their parameter tuning
MPI-I-2005-4-006	C. Fuchs, M. Goesele, T. Chen, H. Seidel	An emperical model for heterogeneous translucent objects
MPI-I-2005-4-005	G. Krawczyk, M. Goesele, H. Seidel	Photometric calibration of high dynamic range cameras
MPI-I-2005-4-004	C. Theobalt, N. Ahmed, E. De Aguiar, G. Ziegler, H. Lensch, M.A. Magnor, H. Seidel	Joint motion and reflectance capture for creating relightable 3D videos
MPI-I-2005-4-003	T. Langer, A.G. Belyaev, H. Seidel	Analysis and design of discrete normals and curvatures
MPI-I-2005-4-002	O. Schall, A. Belyaev, H. Seidel	Sparse meshing of uncertain and noisy surface scattered data